Heliyon 8 (2022) e08805

Contents lists available at ScienceDirect

Heliyon

journal homepage: www.cell.com/heliyon

Research article

Apium graveolens reduced phytofabricated gold nanoparticles and their impacts on the glucose utilization pattern of the isolated rat hemidiaphragm

Rajasekar Panchamoorthy *, Udayamathi Mohan, Anbarasan Muniyan

Department of Biotechnology, Rajalakshmi Engineering College, Thandalam, Chennai, 602 105, Tamil Nadu, India

ARTICLE INFO

Keywords:
Apium graveolens
Gold nanoparticles
Biocompatibility
Glucose uptake
Hemidiaphragm
Molecular docking

ABSTRACT

The integration of nanotechnology with herbal medicines overcomes the limitations of herbal therapy and offers desirable bioactivity. Thus, this study was aimed at synthesizing *Apium graveolens*-gold nanoparticles (AG-AuNPs) and exploring their impact on the glucose utilization pattern of the isolated rat hemidiaphragm. The AG-AuNPs appeared in cherry red color and showed a plasmonic peak at 534nm. The bio-reduced AG-AuNPs appeared as spherical shapes with varying sizes of about 4–15 nm. It also depicted the zeta potential of -19.5 mV, face-centered cubic crystalline nature, stretching vibrations for different functionalities, and *in vitro* stability during various characterization studies. The AG-AuNPs showed non-cytotoxicity and promoted cellular glucose uptake on their exposure to the cell line and the diaphragm, respectively. Moreover, the identified flavonoids and polyphenols of AG depicted *in silico* interactions with the insulin signaling molecule. The observed results suggest that the interacting ability of AG-AuNPs with the insulin signaling molecule can promote the glucose uptake efficiency of the diaphragm.

1. Introduction

Apium graveolens (AG; Family: Apiaceae/Umbelliferae) commonly called celery is mainly used in food for its aromatic taste and smell. It is rich in numerous phytochemicals (flavonoids, polyphenols, glycosides, etc.), vitamins, and minerals. However, the composition and concentration of phytochemicals in celery can vary due to genotypic and environmental differences (Mezeyová et al., 2018). Traditionally, it is used to treat various health problems. It has shown various pharmacological actions including anti-inflammatory, antiradical, antidiabetic, anticoagulant, antimicrobial, anti-cancer, hypolipidemic, hypoglycemic, hypocholesterolemic, hepato, and neuroprotective actions (Prasathkumar et al., 2021; Chonpathompikunlert et al., 2018; Kooti et al., 2015; Shivashri et al., 2013). It demonstrates that AG is a potent herbal plant for several health-related problems.

Moreover, one of the major limitations of herbal therapeutics is poor absorption and distribution to the defective sites, which are due to the alterations in their physicochemical and biochemical properties such as low solubility, reduced absorption, rapid metabolism, and excretion. Furthermore, the bioavailability also depends upon the size of therapeutic compounds. For example, the therapeutic agent distributed in the bloodstream must be less than 5 mm in size to avoid the formation of aggregates with biological compounds (Singh and Lillard, 2009; Patra et al., 2018). This suggests that herbal medicine with numerous beneficial activities should be used properly to elicit the bioavailability mediated action(s). Therefore, a novel drug delivery approach has been desperately required to overcome the issues linked with herbal therapy.

The metals including silver, gold, palladium, platinum, copper, and zinc are considered as noble metals which play an important role in numerous fields including medicine. Among these, gold has been highly preferred in the field of medicine, because metallic gold compounds/sol have long been used in Indian medicine (Parimalam et al., 2020). Apart from this, the nanoparticles of gold also exhibit several unique properties such as ultra-small size, high surface reactivity/functionalization, inertness, biocompatibility, etc. Gold nanoparticles with reduced size and controlled morphology offer a large surface area for ease of functionalization/coating by organic compounds/ligands for effective targeted drug delivery (Sadalage et al., 2021). Moreover, the gold nanoparticles with increased negative zeta charge can interact with protonated oxygen of phytochemicals under an acidic medium (Omolaja et al., 2021). Furthermore, the tautomeric conversion of flavonoids from their enol form to the keto form can favor the reduction of metal ions and also get adsorbed/functionalized on the surface of metallic nanoparticles (Nayem et al., 2020; Oueslati et al., 2020; Khandel et al., 2018). This infers that the gold nanoparticles with or without surface modification can interact with various drugs/phytotherapeutics and serve as a drug delivery vehicle for

* Corresponding author.
E-mail address: rajasekar.panchamurthy@gmail.com (R. Panchamoorthy).

https://doi.org/10.1016/j.heliyon.2022.e08805
Received 14 August 2021; Received in revised form 15 December 2021; Accepted 17 January 2022

targeting particular cells/tissues. Apart from this, it is also suspected that the surface functionalizing property of gold nanoparticles may overcome drugs removal from blood by the liver and splenic activities (Omolaja et al., 2021). This can prolong the time of circulation of gold nanoparticles/carriers and thereby favor its targeted drug delivery.

Metallic nanoparticles (MNPs) are synthesized through different methods including biological routes. In the biological method, plant extracts/phytochemicals/microbes are used as reductive sources for the synthesis of MNPs (Thanganadar Appapalam et al., 2020; Sunderam et al., 2019; Shen et al., 2019; Abdel-Kareem and Zohri, 2018). The green reducing sources are highly preferred because they offer natural ligands and stabilizing agents for the synthesis of nanoparticles. Furthermore, this approach also offers eco-friendly and cost-effective synthesis (Khandel et al., 2018). Several studies demonstrated the green route derived gold nanoparticles for the validation of various pharmacological, biomedical, and environmental applications (Mai et al., 2021; Khoshnamvand et al., 2020; Ghramh et al., 2019; Mahitha et al., 2013).

Moreover, the green source-derived polysaccharide has been used for the preparation of highly stable platinum nanoclusters, which showed high selectivity and sensitivity for the detection of glucose and glutathione in biological fluids (Dong et al., 2021; Fan et al., 2021). Thus, it can be assumed that phytochemicals reduced metallic nanoclusters/phytofabricated metallic nanoparticles would show high selectivity for the cellular transportation and utilization of glucose. Further, there is no study explaining the synthesis and characterization of the fresh leaf extract of *Apium graveolens* fabricated gold nanoparticles (AG-AuNPs). Also, the effect of AG-AuNPs on glucose utilization efficiency of the isolated rat hemidiaphragm has not been studied so far. However, the dried leaf and stem of *Apium graveolens* reduced gold nanoparticles were used for the study of its *in vitro* antioxidant property and photocatalytic degradation of a toxic organic pollutant, 4-nitrophenol. The same study has been reported with different morphology of gold nanoparticles with varying sizes of about 7–85 nm based on the reaction conditions and nature of the reducing agent (dried leaf and stem extracts) employed (Khoshnamvand et al., 2020). It is well known that the physiochemical properties of metallic nanoparticles depend upon various factors such as reaction condition, nature of reducing source, reaction period, etc (Khan et al., 2019). Thus, the current study has selected the fresh leaf extract of *Apium graveolens* as a reducing source for the synthesis of AG-AuNPs and also examined whether it would produce a stable AG-AuNPs with unique properties like a reduced size and uniform shape with desired biological action. To confirm the proposed hypothesis, the synthesized AG-AuNPs were subjected to extensive physicochemical characterization studies. The phytoconstituents and reducing potential of the AG extract were examined through chromatography analysis. The biocompatibility (stability and cytotoxicity) of AG-AuNPs, the impact of AG-AuNPs on *in vitro* glucose metabolism of the rat's hemidiaphragm and *in silico* interactions of AG phytochemicals with the insulin signaling molecule, phosphatidylinositol 3-kinase (PI3K) were also evaluated.

2. Materials and methods

2.1. Chemicals

The Sigma-Aldrich chemicals [$HAuCl_4$ - Chloroauric acid; MTT - 3-(4,5-Dimethylthiazol- 2-yl)-2,5-Diphenyltetrazolium Bromide; DMEM - Dulbecco's Modified Eagle's Medium; BSA - Bovine serum albumin and insulin] with the purity of >98% were purchased and utilized. The other reagents and chemicals used in this study were of AR (analytical reagent) grade purchased from Himedia chemicals, India.

2.2. Preparation of AG extract

The AG plant was cleaned thoroughly and its leaves were collected. Exactly, 50g of AG leaves were weighed, ground (250 mL double distilled water), and warmed in a water bath (40–45 °C; 15 min). The obtained extract was left at room temperature for cooling. Then, it was filtered and used for further analyses.

2.3. Analysis of AG extract

The aqueous AG extract was subjected to the preliminary analyses of various secondary metabolites [polyphenols, flavonoids, steroids, tannins, terpenoids, carbohydrates, cardiac glycosides, carotenoids, combined anthraquinones, saponin glycosides, proteins, phlobatannins, and free anthraquinones] according to the methods of Evans (2002) and Sofowora (1993).

2.4. Chromatographic analysis of AG

2.4.1. Thin layer chromatographic (TLC) separation of AG

The aqueous extract of AG was (1 mg/mL) prepared and concentrated through the process of evaporation at 40–50 °C. The obtained evaporated layer was dissolved in 5mL of acetone and used for TLC profiling. Briefly, 10 μl of prepared test solution (i.e) acetone extract was applied twice on an aluminium-backed flexible silica TLC plate with a thickness of 0.25 mm (MACHEREY-NAGEL GmbH & Co. KG, Germany). Further, the sample was separated using the mixture of solvents consisting of 8 parts of petroleum ether and 2 parts of acetone. Then, the obtained TLC chromatogram was observed under normal light and R_f was computed and compared with standards.

2.4.2. High-performance liquid chromatography (HPLC) analysis of AG phytochemicals

The HPLC analysis of AG extract was performed [liquid chromatography (LCGC—Agilent); column (4.6 mm × 24 cm); mobile phase (100 parts of methanol, and water and 1 part of phosphoric acid); volume injected 20 μL; UV detection at 270 nm] for the quantitation of its phytochemicals and compared with standards.

2.5. Synthesis of AG reduced gold nanoparticles (AG-AuNPs)

For the synthesis of AG-AuNPs, 1 mM $HAuCl_4$ and AG leaf extract were mixed in the ratio of 10:0.5 and sonicated (135 W & 40 kHz; 30 min) in Omin Ruptor 250-ultrasonic homogenizer to get similar size nanoparticles without aggregation (Lee et al., 2012). Further, the reaction mixture was stirred overnight for AG phytochemicals mediated reduction of gold ions into AuNPs. Finally, AG-AuNPs suspension was centrifuged (5,000 rpm & 10 min) and the obtained supernatant was used in further characterization studies.

2.6. Study of physicochemical properties of AG-AuNPs

2.6.1. Ultra-violet absorption analysis of AG-AuNPs

The suspension of AG-AuNPs was taken and its UV-visible light absorption pattern was monitored in the Perkin Elmer-Lambda 35 UV spectrophotometer.

2.6.2. Morphology and size analysis of AG-AuNPs

The AG-AuNPs were coated on a copper grid in the form of a thin film and were examined for their morphology with size under the TECHNAI 10 Philips-transmission electron microscopy (TEM) at 100 kV.

2.6.3. Elemental analysis of AG-AuNPs

The dried thin layer of AG-AuNPs containing a copper grid was screened under SEM-EDX [Scanning Electron Microscopy (VEGA3-TESCAN) with Energy-Dispersive X-ray Spectroscopy (Bruker, Nano GMBH)] for the identification of gold and other elements.

2.6.4. Determination of zeta potential and particle size of AG-AuNPs

The particle size and zeta potential of the filtered (0.5 μm Millipore filter) AG-AuNPs were examined by using dynamic light scattering (DLS-Zetasizer Ver. 7.03).

2.6.5. Analysis of AG-AuNPs crystalline nature

The crystalline nature of the dried AG-AuNPs was studied under the XRD (X-ray Diffractometer, X'pert PRO-MPD, XDL 3000) with Cu Kβ filter, operated at 30 kV and 100 mA.

2.6.6. Study of infrared absorption of AG and AG-AuNPs

Both AG extract and suspension of AG-AuNPs were subjected to FT-IR analysis (JASCO 460 plus spectrophotometer). Briefly, the extract of AG/AG-AuNPs was mixed with the KBr matrix and recorded the FT-IR spectrum under the frequency range of 4000–500 cm^{-1}.

2.7. Assessment of in vitro biocompatibility of AG-AuNPs and study of their effect on glucose utilization in the isolated rat hemidiaphragm

2.7.1. Analysis of AG-AuNPs stability

Different mediums such as 10% sodium chloride (NaCl), 0.5% bovine serum albumin, cysteine (0.2 M), histidine (0.2 M), and varied pH (highly acidic pH 1.2, acidic pH 5, physiological pH 7.4 & alkaline pH 9) of phosphate buffer were taken for the stability analysis of AG-AuNPs. Briefly, the equal volume of AG-AuNPs and individual physiological solution/phosphate buffer solution were mixed and incubated at 37 °C for 24 h. Finally, the UV-Visible light absorption pattern of the incubated mixture was recorded in PerkinElmer, Lambda 35.

2.7.2. Cytotoxicity assay

The lung cancer cell line (A549) was obtained from National Centre for Cell Science (NCCS) Pune, India. The cells were grown in T25 flasks containing DMEM supplemented with 1mM sodium pyruvate, 10% heat-inactivated fetal bovine serum, and 1% antibiotics. The cells were maintained in a humidified incubator at 37 °C with 5% CO_2 and 95% air.

The cytotoxicity assay involves the conversion of yellow-colored MTT to purple formazan by the metabolically active cells. Briefly, 5×10^4 A549 lung cancer cell line was introduced to 96-well plates and maintained in a CO_2 incubator for 24 h. Then, the old medium was replaced with a fresh medium (100 μL/well) containing different (20, 40, 60, 80, and 100 μM) concentrations of gold nanoparticles and incubated again for another 24 h. For the control, A549 cells were not treated with any of the compounds. After the period of incubation, the old medium was removed from both treated and untreated wells, and then MTT was added (5 mg of MTT dissolved in 5 mL of PBS; 50 μL/well) and incubated for a short period (4 h). Finally, MTT was removed from the wells and subsequently mixed with DMSO (dimethyl sulfoxide, 200 μL). The purple color developed was measured by using an ELISA reader (Model 680, Biorad) at 570nm.

2.7.3. Glucose utilization assay

For this assay, the control rats' hemidiaphragms were removed [Institutional Animal Ethics Committee (IAEC) Approval No: SU/CLAR/RD/013/2015] and kept in the prepared solution [sodium phosphate (0.04 M; pH 7.2), potassium chloride (0.005 M), magnesium chloride (0.004 M), and sodium chloride (0.083 M)]. For this assay, the moisture content of the diaphragm was removed by using filter paper. Further, the diaphragm was weighed and placed in the tubes containing the same medium supplemented with glucose (0.006 M). The following series of assay tubes such as hemidiaphragm without AG-AuNPs, AG, and insulin [i.e. control assay tubes for the measurement of glucose utilization under basal condition] and with AG-AuNPs (60 μM & 80 μM), AG (12.5 mg/mL), and insulin (0.2 U/mL) were processed and kept at physiological temperature (37 °C) for 2 h (Haugaard and Haugaard, 1970). Then, the existed levels of glucose in the assay fluid (i.e.) extent of glucose

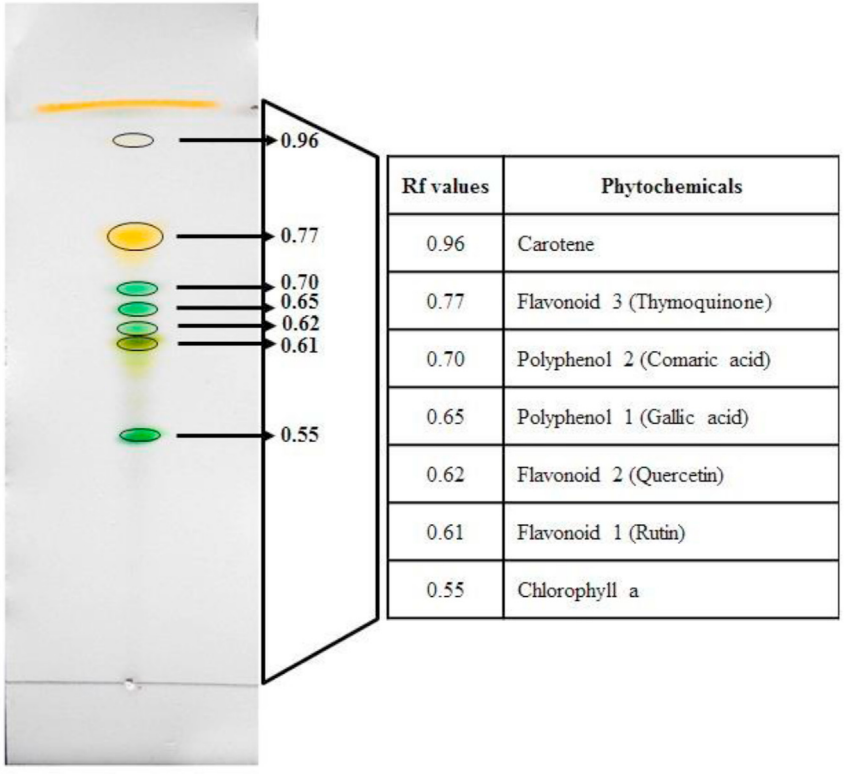

Rf values	Phytochemicals
0.96	Carotene
0.77	Flavonoid 3 (Thymoquinone)
0.70	Polyphenol 2 (Comaric acid)
0.65	Polyphenol 1 (Gallic acid)
0.62	Flavonoid 2 (Quercetin)
0.61	Flavonoid 1 (Rutin)
0.55	Chlorophyll a

Figure 1. Thin layer chromatogram of AG extract. The aqueous extract of AG produced seven distinct bands. The R_f values of these seven bands correspond to the standard R_f values of chlorophyll a, rutin, quercetin, gallic acid, coumaric acid, thymoquinone, and carotene.

utilized by the hemidiaphragm was measured by using glucose oxidase/peroxidase (GOD-POD) reagent. Briefly, 0.01 mL of assay fluid was transferred into the clean test tube and mixed with 1 mL of GOD-POD enzyme reagent and incubated at 37 °C for 15 min. The color developed was read at 510 nm. The glucose uptake by the hemidiaphragm was calculated by the initial and final glucose concentration.

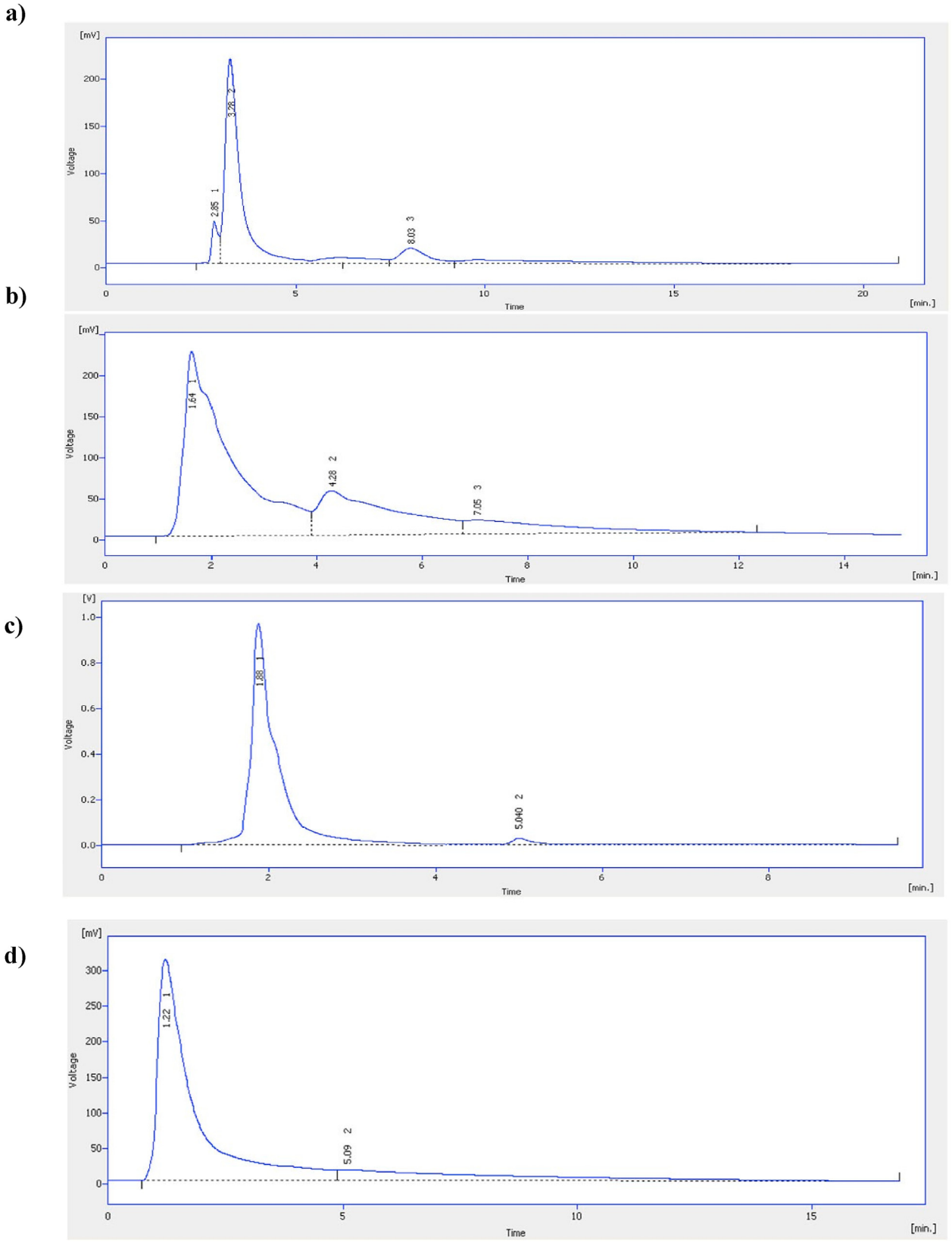

Figure 2. The HPLC chromatogram of a) standard flavonoids, b) AG flavonoids, c) standard polyphenols and d) AG polyphenols.

2.8. Molecular docking analysis

The 3D structure of phosphatidyl inositol-3 kinase (PI3K; Protein Data Bank ID: 2RDO) and the ligands of quercetin, thymoquinone, rutin, coumaric acid, and gallic acid were obtained from PDB databases and PubChem, respectively.

The molecular docking analysis of AG phytochemicals (quercetin, rutin, thymoquinone, coumaric acid & gallic acid) over the insulin signaling molecule, PI3K was carried out using the AutoDock tool. The grid-map energy of the docked protein-ligand complex was obtained from the software (AutoDock). For computing the grid maps, the parameters such as partial charges, solvation, and polar hydrogens were introduced. The affinity map of the protein-ligands and Kollman charges for each atom of the macromolecule were also calculated. Then, the grid box was fixed around the active site amino acids with the spacing of 0.375 Å and performed the cluster analysis by using RMSD (root-mean-square deviation) and Lamarckian genetic algorithm. The most probable solution was obtained from the more populated clusters with the lowest energy conformation. The PyMOL molecular graphics system 1.4.1 was used for the visualization of the docked conformations.

2.9. Data analysis

For the statistical analysis of the obtained data, ANOVA-DMRT (one-way analysis of variance-Duncan's multiple range test) and t-test with different significance levels ($p < 0.0001$; $p < 0.001$; $p < 0.01$ & $p < 0.05$) were followed. The values were denoted as mean ± SD.

3. Results and discussion

3.1. AG phytochemicals

The aqueous leaf extract of AG answered for polyphenols, flavonoids, steroids, tannins, terpenoids, carbohydrates, cardiac glycosides, carotenoids, and combined anthraquinones. Whereas, the AG extract did not answer for saponin glycosides, proteins, phlabotannins, and free anthraquinones.

The TLC separation of AG extract produced seven distinct bands (Figure 1). More interestingly, further phytochemical analyses revealed that the separated bands contained flavonoids and polyphenols. Furthermore, the obtained R_f values of the separated bands were similar to the R_f values of phytochemicals such as rutin, quercetin, gallic acid, coumaric acid, and thymoquinone, confirming that the prepared AG extract was enriched with polyphenols and flavonoids contents.

Based on the preliminary identification of the phytochemicals of AG extract, further study quantitated the levels of thymoquinone, quercetin, rutin, gallic acid, and coumaric acid in the extract by using HPLC. In the obtained HPLC chromatogram, three different peaks were noticed and their retention times were found to be 1.64, 4.28, & 7.05 min, respectively, which were similar to the noticed retention time of the flavonoid standards such as quercetin, rutin, and thymoquinone (Figure 2 a & b). The levels of quercetin, rutin, and thymoquinone in the fresh leaf extract of AG were found to be 5.49 ± 0.705, 13.4 ± 0.635, & 2.302 ± 0.637, mg/mL respectively.

The AG extract also generated two distinct peaks with the retention time of 1.22 min and 5.09 min, respectively. These were matched with

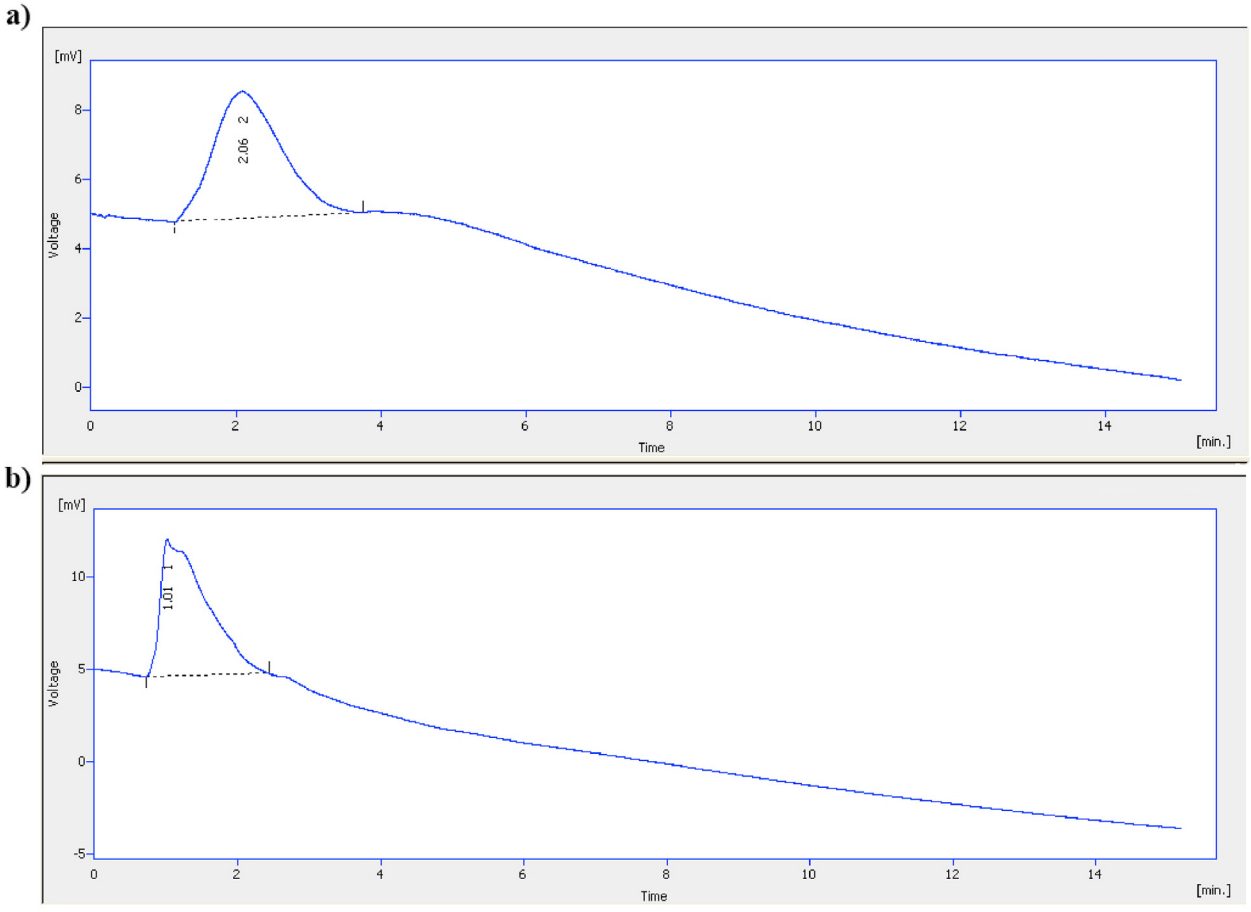

Figure 3. The HPLC chromatogram of a) flavonoids and b) polyphenols in AG-AuNPs.

the retention time of standard polyphenols such as coumaric acid and gallic acid (Figure 2 c & d). The concentrations of coumaric acid and gallic acid in the AG extract were found to be 16.2 ± 0.732, & 3.6 ± 0.61, mg/mL respectively. Further, the observed chromatogram results confirmed the enrichment of multiple phytochemicals in the aqueous leaf extract of AG. The flavonoid, quercetin and polyphenol, coumaric acid have been previously identified in the plant celery (Zhou et al., 2009; Mutha et al., 2021). But, this study identified other flavonoids (rutin & thymoquinone) and polyphenols (gallic acid & coumaric acid) in the fresh leaf extract of AG.

3.2. Preliminary and spectral confirmation of AG-AuNPs

3.2.1. Color and UV absorption of AG-AuNPs & reducing efficiency of AG

Figure 4 depicts a) the color and b) the UV-visible absorption pattern of AG-AuNPs. The reaction of $HAuCl_4$ with the aqueous fresh leaf extract of AG produced cherry red color after 24 h, which showed a characteristic absorption at 534 nm, demonstrating the AG phytochemicals mediated bioreduction of Au^{3+} to Au^0. Generally, gold nanoparticles can exhibit either purple, brown, orange, or red in the solution state (Amina and Guo 2020; Santhoshkumar et al., 2017). Gold nanoparticles also show surface plasmon resonance (SPR) band at 500–550 nm. The color and SPR of gold nanoparticles fully depend upon nanoparticles size (Jain et al., 2006). The SPR band of gold nanoparticles is mainly due to the oscillations of conduction electrons induced by the incident photon (Templeton et al., 2000).

To confirm the bioreduction of Au^{3+} to Au^0, the levels of existing phytochemicals were analyzed in the suspension of AG-AuNPs. Interestingly, the peaks for flavonoids such as thymoquinone and quercetin disappeared in the generated HPLC chromatogram of the AG-AuNPs suspension when compared to the chromatogram of AG extract. Whereas, the flavonoid, rutin peak was observed at 2.06 min (Figure 3 a & 2 b). Furthermore, the polyphenols chromatogram of the AG-AuNPs suspension showed the peak for coumaric acid with the disappeared gallic acid peak (Figure 3 b) when compared to the chromatogram of AG (Figure 2 d). The utilized flavonoids (quercetin 100%, rutin 81.79%, & thymoquinone 100%), and polyphenols (coumaric acid 79.63% & gallic acid 100%) in the suspension of AG-AuNPs demonstrated their reducing and stabilizing actions. The completely utilized phytochemicals such as quercetin, thymoquinone, and gallic acid in the suspension of AG-AuNPs confirmed their fabricating (i.e) surface functionalizing efficiency on the surface of gold nanoparticles (Figure 4 c). Our findings are in line with the statement of previous studies that explained the green products and the antioxidants of extracts can act as reducing and stabilizing agents for the synthesis of metallic nanoparticles. Especially, the prepared gold nanoparticles have exhibited medicinal properties (Lee et al., 2020; Jia et al., 2009). In addition, the plant extract also facilitated the synthesis of nanoparticles through its reducing and stabilizing actions (Selvakumar and Rajasekar 2017).

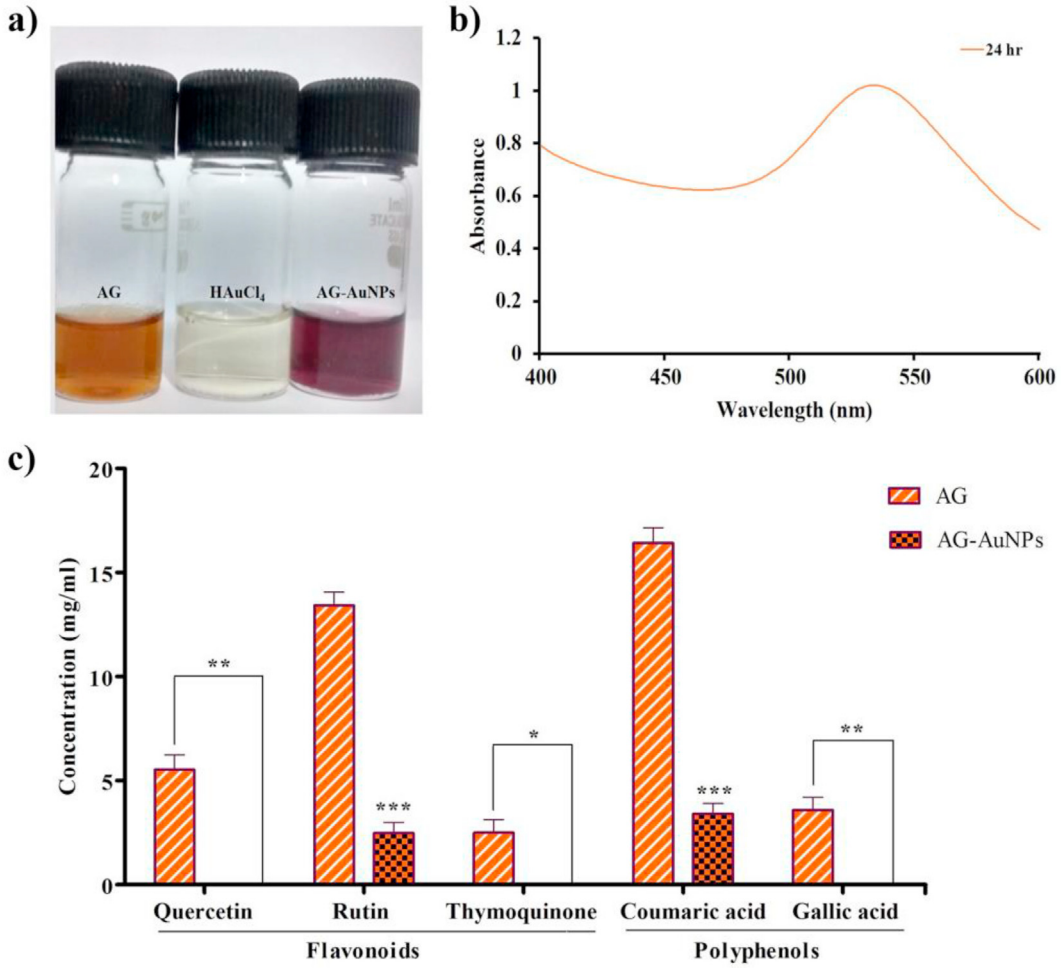

Figure 4. a) The color of AG (brown), $HAuCl_4$ (pale yellow), and AG-AuNPs (cherry red). b) The UV-visible absorption pattern of AG-AuNPs. The reduced gold nanoparticles displayed maximum absorption at 534 nm. c) The concentration of AG phytochemicals before (AG extract) and after synthesis of AG-AuNPs. The obtained triplicates data are expressed in means ± SD. The results of the groups were analyzed by the Student's 't' test. The significance levels were marked at the different p values such as ***$p < 0.001$, **$p < 0.01$, & *$p < 0.05$. AG- *Apium graveolens*; AG-AuNPs- *Apium graveolens* fabricated gold nanoparticles.

3.3. Morphology, elemental distribution, particle size, zeta-charge, and crystalline nature of the bio-reduced gold nanoparticles

The TEM micrographs of AG-AuNPs depicted a spherical morphology & sizes 4–15 nm (Figure 5a & 5a inset). Furthermore, the obtained EDAX spectrum of AG-AuNPs showed the characteristic gold peak at 2.12 keV. In addition, another gold peak was observed at 0.26 keV along with the peaks for carbon (0.28 keV) and oxygen (0.53 keV) (Figure 5b), demonstrating the fabricated AG phytoconstituents on the surface of AuNPs.

The exposure of leaf extract of *Coriandrum sativum* (family: Apiaceae) and a dried leaf and stem extracts of *Apium graveolens* with the gold ions solution developed the AuNPs with different morphologies like a triangle, spherical decahedral, and truncated triangles (Khoshnamvand et al., 2020; Santhoshkumar et al., 2017). Furthermore, the slow reduction of gold ions by carbonyl compound of plant extract has exerted a shape-controlling effect and thereby developed gold nanotriangles (Azizi et al., 2013). In the current study, the monodispersed spherical shaped nanoparticles were observed under the TEM analysis of the fresh leaf extract of AG fabricated gold nanoparticles and this could be influenced by various factors including the nature of reducing source, reaction time and conditions followed, etc (Khan et al., 2019).

Figure 5 c-d) illustrates the particle size and zeta-charge of AG-AuNPs. The analysis of AG-AuNPs using DLS produced a spectrum with three distinct peaks. But, the intensities of the first two peaks were very low when compared to the intensity of the third peak. Therefore, the average hydrodynamic size of AG-AuNPs was found to be 69.98 nm (Figure 5 c). This result revealed that the average particle size of AG-AuNPs suspension was increased compared to, the sizes (4–15 nm) which were observed under TEM measurement. This size variation could have been influenced by the physical nature of the sample used in DLS & TEM analyses and the nature of the reducing source employed for the synthesis of AG-AuNPs. For example, the dried plant materials (leaf and stem) of *Apium graveolens* reduced gold nanoparticles have shown increased hydrodynamic size under DLS analysis (Khoshnamvand et al., 2020; Eaton et al., 2017). It has been demonstrated that the stability of metallic nanoparticles in the solution state is fully dependent upon their zeta-charge. It is mainly determined by the surface integrated compounds. For example, metallic nanoparticles with a surface charge of either more negative (<-30) or more positive (<+30) have depicted superior stability (Adena et al., 2019). This study has noted the zeta charge of -19.5 mV for the synthesized AG-AuNPs (Figure 5d), illustrating their remarkable structural stability in the medium. The surface-attached/interacting flavonoids and polyphenols of AG might have contributed more negative charge to AG-AuNPs. Thus, the negatively charged AG-AuNPs could exert a repulsive force between the dispersed phase and dispersion medium for the maintenance of stability (i.e.) the establishment of a repulsive force between the dispersed phase and dispersion medium could have prevented the agglomeration-mediated instability of AG-AuNPs (Amina and Guo 2020).

3.4. The XRD and FT-IR spectra of AG-AuNPs

In the XRD spectrum of AG-AuNPs, four distinct peaks were observed at the angles of 38.01°, 44.88°, 64.43°, and 77.40° which were related to Bragg refractions planes (111) (200), (220), & (311), respectively (Figure 6 a). The obtained results demonstrated that AG-AuNPs resembled the face-centered cubic (fcc) lattices of gold and were of crystalline nature. The XRD data of AG-AuNPs are in agreement with others'

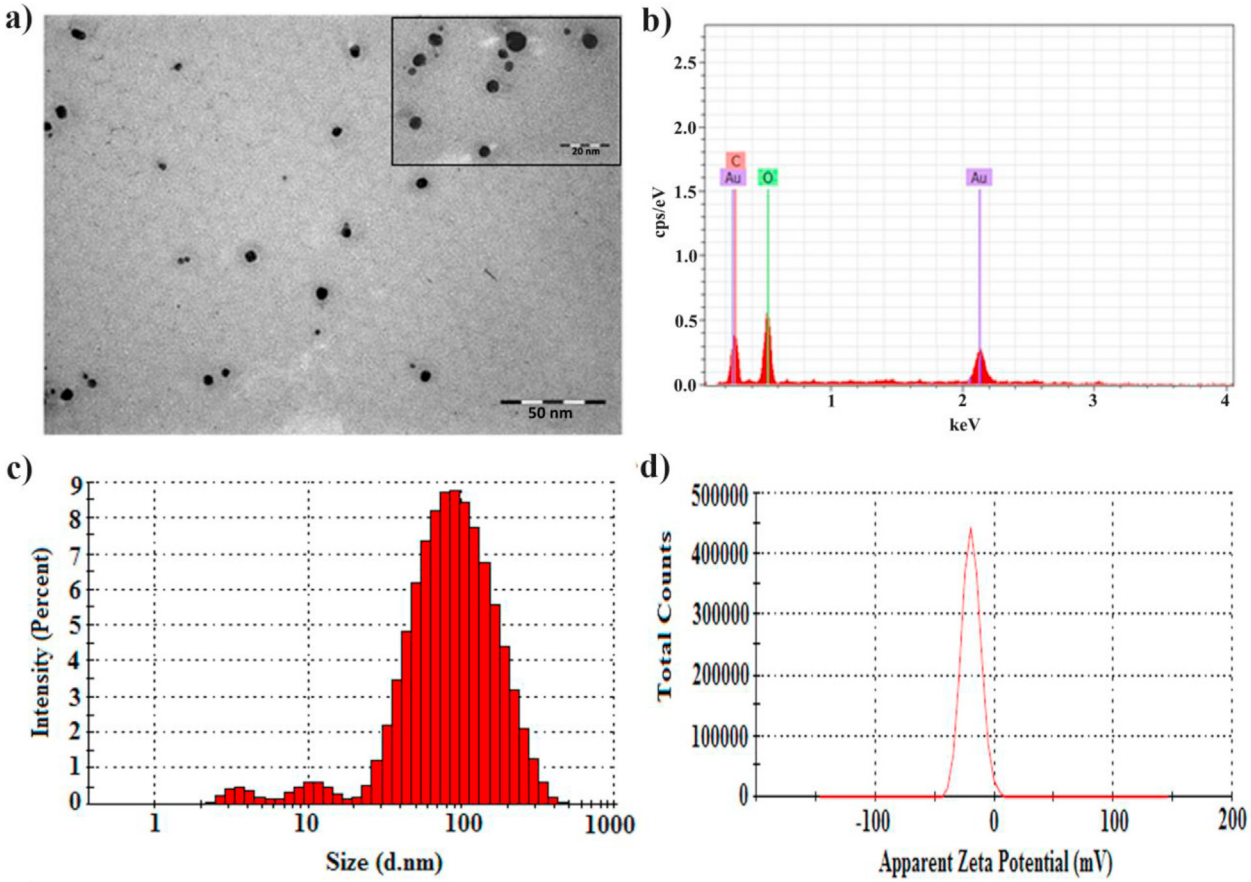

Figure 5. a) The morphology, b) elemental distribution, c) particle size, and d) zeta-charge of AG-AuNPs. The gold nanoparticles appeared spherical morphology with sizes of 4–15 nm. The EDX spectrum of AG-AuNPs showed the signals for elemental gold, carbon, and oxygen. In addition, the AG-AuNPs suspension also showed an average particle size of 69.98 nm, and a zeta-charge of -19.5 mV during DLS analysis.

findings (Sett et al., 2016; Babu et al., 2016; Zhao et al., 2018; Abdoli et al., 2021). However, the presence of additional grains/peaks along with the characteristic crystallographic planes of gold at 2θ values (30–80 °) might have resulted from the bio-organic compounds of plant extract employed during the synthesis (Gardea-Torresdey et al., 2002). Furthermore, the existence of additional peaks/grains at 2θ values did not affect the characteristic crystallographic planes of gold. Additionally, this could play a role in the structural stability of gold nanoparticles.

Figure 6 b & c gives the infrared absorption pattern of AG and bio-reduced gold nanoparticles. In this study, the infrared absorption spectrums of AG and AuNPs were recorded and compared further to confirm the AG functionalities mediated bioreduction of gold ions into AuNPs. The AG depicted stretching vibrations between 3433 to 1177 cm^{-1} for different functionalities such as O–H, =C–H, C=O, C=C, and C–O, and the specific stretching vibrations of these groups were observed at the frequencies of 3433, 3083, 3000, 1698, 1482, 1374 & 1177 cm^{-1}, respectively. In addition, the frequencies of = C–H out of plane deformation and = C–H bending were also observed from 929 to 459 cm^{-1} (Figure 6 b).

The infrared absorption pattern of AG-AuNPs revealed a lower wavenumber for –OH stretching (3400 cm^{-1}) (Figure 6 c). It has been observed that a strong stretching vibration peak for the phenolic OH group of quercetin (3370 cm^{-1}) got shifted to a lower wavenumber in the quercetin functionalized AuNPs, and suggested the hydroxyl group of quercetin interacted/associated on the surface of gold nanoparticles (Das et al., 2013). Furthermore, the reduction of $HAuCl_4$ by the phytochemical rutin formed the red-colored rutin-AuNPs. Apart from this, the primary alcohols, diols, polyols, dextrin, and cellulose can also reduce $HAuCl_4$ to AuNPs (Levchenko et al., 2011). This suggests that the hydroxyl group of quercetin and rutin of AG extract could reduce the gold ion into gold nanoparticles.

This study observed the higher wavenumbers for the C=O, C=C, C–O, and = C–H functionalities, and their increased frequencies were 1724, 1539, 1260, and 961 cm^{-1}, respectively (Figure 6 c). It has been explained that an organic acid with the hydroxyl group functionality can stabilize the AuNPs either at low pH or high pH. For example, at high pH, the stabilizing nature of gallic acid has been attributed through its hydroxyl group, whereas, at low pH, the carboxyl group of gallic acid gets bound with AuNPs (Moreno-Álvarez et al., 2010). In addition, the grape leaves extract reduced AuNPs have shown a medium intense FT-IR band for the C=O stretching and suggested that the COOH group-containing compound (i.e.) C=O group does not interact with AuNPs (Iyer and

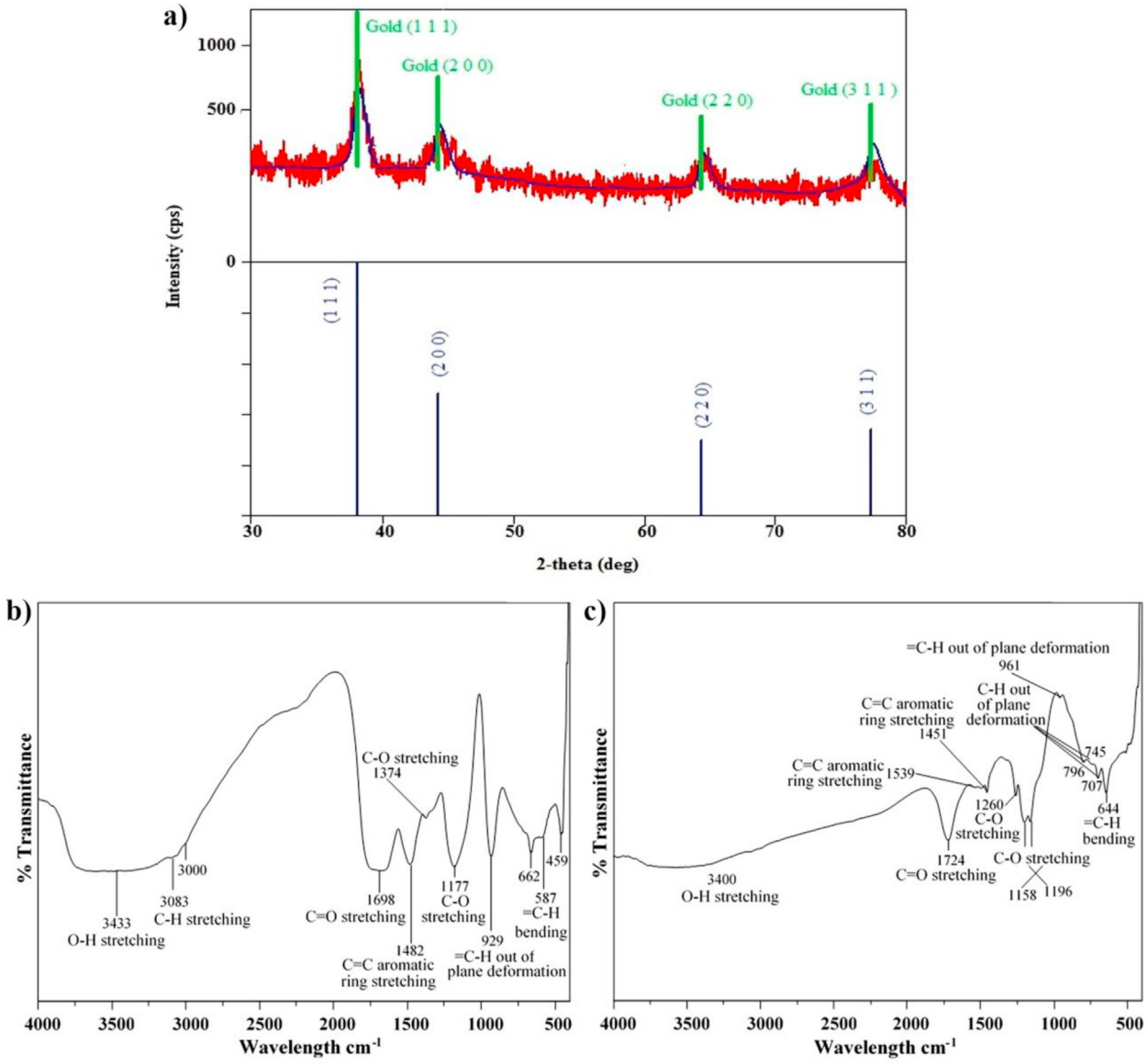

Figure 6. a) The XRD and b & c) FT-IR spectra of AG and AG-AuNPs. The AG-AuNPs display a face-centered cubic (fcc) crystalline nature under XRD analysis. AG-*Apium graveolens*; AG-AuNPs- *Apium graveolens* fabricated gold nanoparticles.

Panda 2018). Furthermore, it has been studied that the increasing palladium II concentration in the palladium-polyvinyl pyrrolidone nanoparticles solution, promotes the polyvinyl pyrrolidone (PVP)–CO signal to higher wavenumber, and suggested that a weaker interaction mediated release of adsorbed PVP from the palladium surface (Nemamcha et al., 2006). From the decreased coumaric acid concentration in the AG-AuNPs suspension and increased wave number for C=O, it can be strongly believed that the bioreduced gold nanoparticles were functionalized by coumaric acid through its hydroxyl group with the projection of its free carbonyl group.

Furthermore, the disappearance of peaks for = C–H (stretching), C–O, and = C–H (bending), and the existence of additional peaks for C=C and = C–H were also noticed in the spectrum of AG-AuNPs (Figure 6 c). The disappeared stretching wavenumbers for = C–H and C–O peaks were found at 3083, 3000, and 1374 cm $^{-1}$, respectively. The frequencies for aromatic stretching (C=C; 1451cm^{-1}), out plane deformation (=C–H; 796, 745, 707 cm^{-1}), and bending (=C–H; 644 cm^{-1}) also exist in the IR data of AG-AuNPs (Figure 6 c). This study also observed the complete utilization of gallic acid in the suspension of AG-AuNPs, which provided clear evidence for its reducing and stabilizing properties (Naz et al., 2014). Apart from this, it has been explained that gallic acid can reduce chloroauric acid and thereby produce AuNPs and quinoid forms of gallic acid. Further, the quinoid forms of gallic acid can eventually get adsorbed on the surface of gold nanoparticles (Wang et al., 2007). This confirms that the reduction of $HAuCl_4$ to Au^0 could be mediated by quercetin, rutin, thymoquinone, and gallic acid and the stability of AG-AuNPs could be established through gallic acid and coumaric acid of AG. Furthermore, it is also evident that the carboxylic acid group of gallic acid and coumaric acid might contribute to the zeta-charge of AG-AuNPs.

3.5. Biocompatibility and in vitro tissue glucose utilizing action of the AG-AuNPs

3.5.1. Stability of AG-AuNPs

The biocompatibility of any therapeutic formulation is evaluated through key parameters such as stability, cytotoxicity, and cell viability. For example, the dispersion stability of metallic nanoparticles is affected by various factors including pH, salt concentration, etc (Zhang et al., 2012). Thus, the strategies like thiolation, cyclic poly (ethylene glycol) physisorption, and preservation in citrate solution have been followed for the improvement of dispersion stability of metallic nanoparticles, especially for biomedical applications (Wang et al., 2020b; Kralik, 2014). It is well known that the physiological medium contains plenty of different electrolytes that can eventually affect the charge and structural integrity of nanoparticles (Pamies et al., 2014). As this study involved the synthesis of phytofabricated gold nanoparticles through the green route approach, the dispersion stability of AG-AuNPs was examined in the selected medium (BSA, sodium chloride, cysteine & histidine), and phosphate buffer solution of varied pH (highly acidic, acidic, physiological & alkaline pH). The incubation of AG-AuNPs with different mediums showed an increased shift (~2–12 nm) in their plasmon wavelength (534 nm) (Figure 7 a & b). But, the maximum of increased shift (i.e. 546 nm) was observed during the exposure of AG-AuNPs in the high ionic strength solution (10% NaCl) and buffer solution with highly acidic pH (pH 1.2), demonstrating the alteration of AG-AuNPs behavior in the high strength of ionic and acidic conditions. However, the exposed AG-AuNPs in the buffer solution with pH 7.4 produced 2 nm shifts (i.e 536 nm) in their characteristic wavelength of 534 nm, indicating the structural integrity of AG-AuNPs in the physiologically relevant medium.

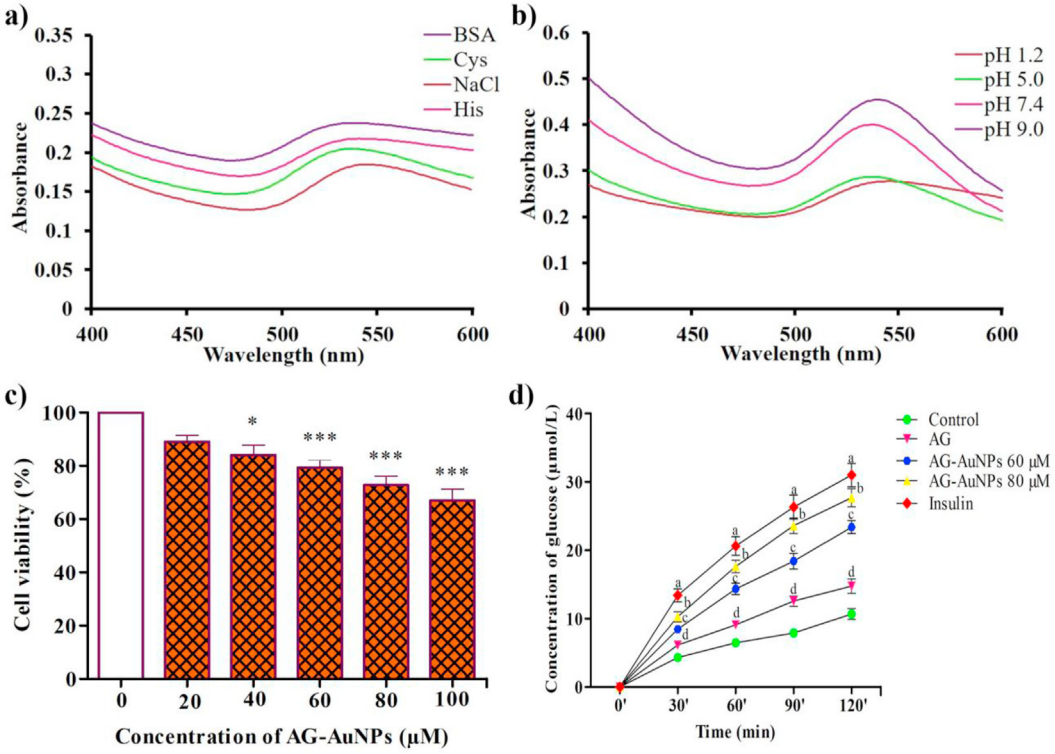

Figure 7. a & b) The *in vitro* stability and c) cytotoxicity of AG-AuNPs. a & b) The fabricated AG-AuNPs showed a 2–12 nm shift in their surface plasmon resonance on incubation with the different medium. c) The AG-AuNPs of different concentrations (20, 40, 60, 80 & 100 µM) displayed non-cytotoxicity on A549 cells. The obtained data are expressed in means ± SD. n = 3. The results of the groups were analyzed by the Student's 't' test. The significance levels were marked at the different p values such as *p < 0.05 and ***p < 0.001. d) The impact of AG-AuNPs on the glucose uptake of the isolated rat hemidiaphragm. The pattern of glucose utilization increased based on the concentrations of AG-AuNPs used. The results of the groups were analyzed by using one-way ANOVA-DMRT. The significance level was noted at the p-value of ^{a,b,c,d}p<0.0001. ^{a}-compared to control; AG-AuNPs (60 & 80 µM), and AG; ^{b}-compared to control and AG; ^{c}-compared to control and AG; ^{d}-compared to control, insulin and AG-AuNPs (60 & 80 µM). AG- *Apium graveolens*; AG- AuNPs- *Apium graveolens* fabricated gold nanoparticles.

3.5.2. Non-cytotoxicity of AG-AuNPs

Biocompatibility of materials has been assessed through their stability analysis and cytotoxicity or cell viability assay. The MTT assay has been widely used to determine cytotoxicity or cell viability (Mosmann, 1983). The degree of biocompatibility depends on the nature of bioapplications, even if more than 90% is considered as the better range of biocompatibility (Li et al., 2008). Furthermore, the cytotoxic potential of samples has been assessed through the following intensity scales: 1) Cell growth inhibition lower than 50%, inferring no cytotoxicity. 2) The cell growth inhibition level falls between 70 and 90%, representing moderate cytotoxicity. 3) The inhibition of cell growth ranges from 95 to 100%, indicating complete cytotoxicity (Rodrigues et al., 2014).

It has been demonstrated that the incubation of L929 cells with a higher concentration of zinc oxide nanotube has reduced the viability to approximately 50%. This suggested that the concentration of zinc oxide nanotube lower than 100 μg/ml is considered completely biocompatible and biosafe (Li et al., 2008). Moreover, the folic acid conjugated silica @gold core-shell nanoparticles (FA-SiO_2@AuNPs) depicted no significant cytotoxicity in human dermal fibroblast (HDF) cell lines, whereas the viability of A375 cells got reduced about 31% and 16% on incubation with SiO2@Au and FA-SiO2@AuNPs, respectively (Majidi et al., 2019). Similarly, in another study, it was observed that hesperidin loaded gold nanoparticles (size 40 nm and zeta charge -29.40 mV) displayed remarkable cytotoxicity against the breast cancer MDA-MB-231 cell line and non-cytotoxicity (cell viability of approximately 86% at 125 μg/ml) against the normal human HBL cell line (Sulaiman et al., 2020). In addition, the aqueous leaf extract of *Centaurea behen* reduced gold nanoparticles with size between 20 and 50 nm also displayed cytotoxicity against the cancer cell line (THP-1) and non-cytotoxicity over normal cell line (HUVEC) (Abdoli et al., 2021). The citrate stabilized AuNPs displayed poor cell viability when compared with the AuNPs stabilized with gum arabic and starch. This suggested the acidic character of citrate (i.e)

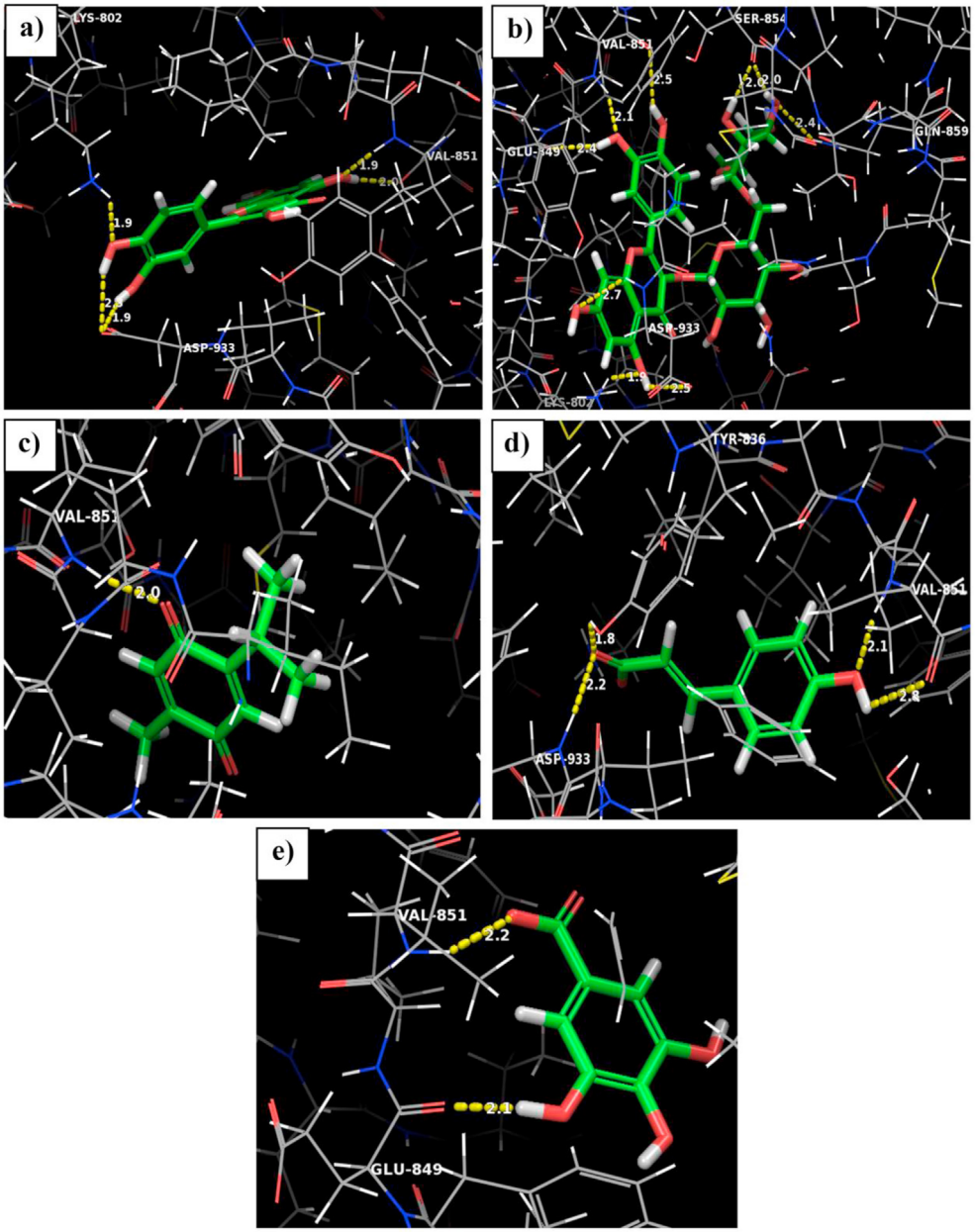

Figure 8. The docking images of AG bioactive compounds with PI3K. a-e) PI3K + quercetin, rutin, thymoquinone, coumaric acid, & gallic acid, respectively. PI3K-Phosphatidylinositol 3-kinase.

the nature of stabilizing agent could determine the cytotoxic property of AuNPs (Vijayakumar and Ganesan 2012). It evinces that the cytotoxicity/poor cell viability of nanomaterials can be determined by the nature of cell lines selected and properties of nanomaterials, including size, surface charge, and conjugated compounds.

The present study confirmed the reduced cell viability of the lung cancer cell line (A549) on its incubation with the phytofabricated AG-AuNPs. With respect to the viability (100%) of AG-AuNPs untreated A549 cell line (i.e. control), the different concentrations of AG-AuNPs (20, 40, 60, 80 & 100 μM) exposure reduced the cell viability to various extents such as 11%, 16%, 20.7%, 27.1%, and 33%, respectively (i.e) the different concentrations of AG-AuNPs treated cell line showed the viability of 89%, 84%, 79.3%, 72.9% & 67%, respectively (Figure 7 c). This study observed above 50% cell viability (i.e. 67%) at the highest concentration of AG-AuNPs exposed cancer cell line. In line with the reports of Li et al. (2008) and Rodrigues et al. (2014), this study confirmed the non-cytoxic nature of AG-AuNPs and also considered the lower concentrations of AG-AuNPs such as 60 and 80μM for the further *in vitro* study.

3.5.3. Effect of AG-AuNPs on the glucose uptake of the isolated rat hemidiaphragm

The isolated rat hemidiaphragm is considered as a reliable tissue for the study of *in vitro* peripheral glucose uptake in the presence of various compounds, including insulin, plants extracts, phytochemicals, etc. Because, it has insulin receptors and machinery for cellular glucose transport (Zierath and Henriksson 2003; Wang, 1985). Furthermore, *the in vitro* approach also offers several advantages such as simplicity, reliability, and reproducibility of the experimental setup/results (Moleiro et al., 2017). Thus, the present study explored *in vitro* glucose uptake efficiency of the hemidiaphragm in the presence or absence of AG-AuNPs/AG extract/insulin (Figure 7 d). Interestingly, the diaphragm incubated with the AG-AuNPs (60 μM & 80 μM) displayed concentration-dependent increased glucose utilization at different time points when compared to the untreated control diaphragm, and AG extract-treated diaphragm. More prominent glucose utilization was observed when the diaphragm was exposed to insulin supplemented medium. However, the higher concentration of AG-AuNPs (80 μM)

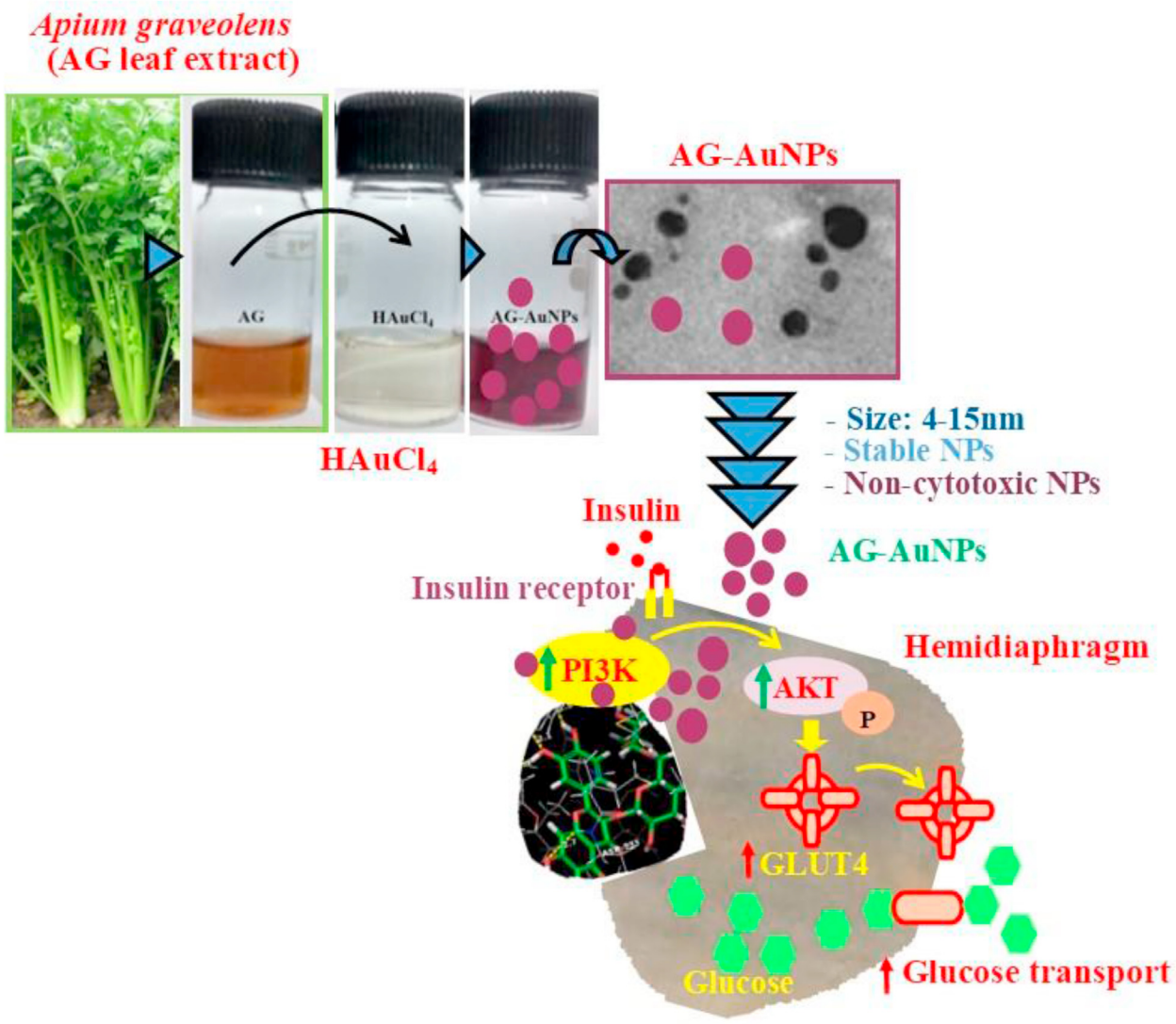

Scheme 1. The proposed glucose utilization mechanism of AG-AuNPs in the isolated rat hemidiaphragm. The leaf extract of *Apium graveolens* fabricated stable, non-cytotoxic, and monodispersed gold nanoparticles with reduced size promoted the *in vitro* glucose uptake in the isolated rat hemidiaphragm. The phytochemicals of *Apium graveolens* showed *in silico* interaction with the key insulin signaling molecule, PI3K. These findings suggested that the interaction of AG-AuNPs with PI3K could potentiate post-receptor signaling for the translocation of GLUT4 vesicle from the cytosolic phase into the membrane, which eventually increased the glucose uptake in the isolated rat hemidiaphragm. AG - *Apium graveolens*; AG-AuNPs - *Apium graveolens* fabricated gold nanoparticles; PI3K - Phosphoinositide 3-kinase; AKT - protein kinase B/AKT; GLUT4 - Glucose transporter type 4.

displayed a closely similar pattern of glucose disposal like that of insulin, confirming its regulatory effect(s) on the tissue glucose metabolism. This is the first report explaining the *in vitro* peripheral tissue glucose utilizing action of AG-AuNPs.

The phytochemicals such as rutin and quercetin and plant extracts have shown enhanced glucose uptake in the rat diaphragm (Lankatillake et al., 2019; Jadhav and Puchchakayala 2012). Apart from this, gallic acid, a polyphenol has displayed the increased translocation of glucose transporter 4 (GLUT4) in 3T3 L1 adipocytes for the promotion of glucose utilization (Wang et al., 2020). Furthermore, the multiple biological actions of thymoquinone have been confirmed for the validation of its antidiabetic property (Abdelrazek et al., 2018). It infers that the bioactive phytochemicals and plant extracts can induce/stimulate cellular machinery for the increase in glucose transport and its utilization. In the present study, the well-characterized AG-AuNPs (sizes: 4–15 nm) might interact with critically important signaling molecules/cellular machinery and thereby promote the sensitivity and selectivity of the hemidiaphragm for the utilization of glucose from the medium.

3.6. Interaction of AG phytochemicals with PI3K

This study also performed the molecular docking of AG phytochemicals with PI3K (Figure 8 a-e). Interestingly, flavonoids of AG such as quercetin (−9.627 kcal/mol; Figure 8 a), rutin (−12.41 kcal/mol; Figure 8 b), and thymoquinone (−6.146 kcal/mol; Figure 8 c) displayed strong interactions with PI3K. Similarly, the polyphenols such as coumaric acid (Figure 8 d) and gallic acid (Figure 8 e) also interacted with the binding sites of PI3K with the binding energy of -6.62 kcal/mol and 6.253 kcal/mol, respectively.

Rutin showed hydrogen bonding interactions with amino acids of PI3K such as Asp 933, Glu 849, Gln 859, Lys 802, Ser 854, and Val 851. But quercetin and thymoquinone showed three (Lys 802, Asp 933 & Val 851) and one (Val 851) interaction with the active site amino acids of PI3K, respectively. Additionally, coumaric acid and gallic acid also displayed binding interaction with the active site of PI3K through Val 851 and Asp 933 and Glu 849 and Val 851, respectively. It is also noticed that all of the ligands showed a common docking interaction with PI3K through Val 851. The observed *in silico* interactions of the identified flavonoids and polyphenols of AG with PI3K imply the positive impacts of phytofabricated gold nanoparticles on the critically important insulin signaling molecule, PI3K.

The PI3K has been considered as an important signaling molecule for insulin signaling mediated cellular glucose uptake. For example, the arresting of the PI3K-Akt signaling leads to inhibiting the membrane translocation of GLUT4 and glucose transport (Liu et al., 2018). It is also confirmed that the polyphenols of coffee by-products regulate the insulin/PI3K/signaling pathways and thereby normalized insulin resistance, mitochondrial dysfunction, adipogenesis, and associated inflammation (Rebollo-Hernanz et al., 2019). Moreover, the dietary flavonoids also induced glucose utilization in the soleus muscle of rats through their regulatory effects over PI3K (Mokashi et al., 2017). This infers that PI3K is a critical signaling molecule for cellular glucose uptake and also a target for the study of the impact of hypoglycemic agents. Interestingly, all the identified flavonoids and polyphenols of AG displayed very effective interactions over the binding pocket residues of PI3K, suggesting that the nanonization mediated delivery of bioactive phytochemicals might have freely interacted with the insulin signaling molecule like PI3K. Further, the PI3K signaling mediated post-receptor signaling events could be eventually promoted the sensitivity and selectivity for the transport and utilization of glucose in the isolated rat diaphragm (Scheme 1).

4. Conclusions

The aqueous leaf extract of *Apium graveolens* reduced gold nanoparticles with sizes of about 4–15 nm showed remarkable biocompatibility in terms of structural stability and non-cytotoxicity. It also promoted the glucose uptake of the isolated rat hemidiaphragm under *in vitro* conditions. Apart from this, the identified polyphenols and flavonoids of *Apium graveolens* showed remarkable *in silico* interactions with the active amino acids residues the key insulin signaling molecule, PI3K. The results of this study confirm the positive impacts of AG-AuNPs on tissue glucose utilization under *in vitro* conditions. In addition, further *in vivo* studies are warranted for the validation of exact glucose-lowering and antidiabetic mechanism(s) of AG-AuNPs.

Ethical approval

The animal study was carried out based on the IAEC (Institutional Animal Ethics Committee; Approval No: SU/CLAR/RD/013/2015) guidelines.

Declarations

Author contribution statement

Panchamoorthy Rajasekar: Conceived and designed the experiments; Performed the experiments; Analyzed and interpreted the data; Contributed reagents, materials, analysis tools or data; Wrote the paper.

Udayamathi Mohan, Anbarasan Muniyan: Performed the experiments; analyzed and interpreted the data; Contributed reagents, materials, analysis tools or data.

Funding statement

This work was supported by AICTE-RPS (All India Council for Technical Education Research Promotion Scheme; File No: 8- 164/RIFD/RPS/POLICY-4/2013-140), India.

Data availability statement

Data will be made available on request.

Declaration of interests statement

The authors declare no conflict of interest.

Additional information

No additional information is available for this paper.

References

Abdel-Kareem, M.M., Zohri, A.A., 2018. Extracellular mycosynthesis of gold nanoparticles using *Trichoderma hamatum*: optimization, characterization and antimicrobial activity. Lett. Appl. Microbiol. 67, 465–475.

Abdelrazek, H.M.A., Kilany, O.E., Muhammad, M.A.A., Tag, H.M., Abdelazim, A.M., 2018. Black seed thymoquinone improved insulin secretion, hepatic glycogen storage, and oxidative stress in streptozotocin-induced diabetic male Wistar rats. Oxid. Med. Cell. Longev. 2018, 8104165.

Abdoli, M., Arkan, E., Shekarbeygi, Z., Khaledian, S., 2021. Green synthesis of gold nanoparticles using *Centaurea behen* leaf aqueous extract and investigating their antioxidant and cytotoxic effects on acute leukemia cancer cell line (THP-1). Inorg. Chem. Commun. 129, 108649.

Adena, S.K.R., Upadhyay, M., Vardhan, H., Mishra, B., 2019. Development, optimization, and *in vitro* characterization of dasatinib-loaded PEG functionalized chitosan capped gold nanoparticles using Box-Behnken experimental design. Drug Dev. Ind. Pharm. 44, 493–501.

Amina, S.J., Guo, B., 2020. A review on the synthesis and functionalization of gold nanoparticles as a drug delivery vehicle. Int. J. Nanomed. 15, 9823–9857.

Azizi, S., Ahmad, M., Mahdavi, M., Abdolmohammadi, S., 2013. Preparation, characterization, and antimicrobial activities of ZnO nanoparticles/cellulose nanocrystal nanocomposites. Bioresources 8, 1841–1851.

Babu, S.G., Gopiraman, M., Deng, D., Wei, K., Karvembu, R., Kim, I.S., 2016. Robust Au-Ag/graphene bimetallic nanocatalyst for multifunctional activity with high synergism. Chem. Eng. J. 300, 146–159.

Chonpathompikunlert, P., Boonruamkaew, P., Sukketsiri, W., Hutamekalin, P., Sroyraya, M., 2018. The antioxidant and neurochemical activity of *Apium graveolens* L. and its ameliorative effect on MPTP-induced Parkinson-like symptoms in mice. BMC Compl. Alternative Med. 18, 103–114.

Das, S., Roy, P., Mondal, S., Bera, T., Mukherjee, A., 2013. One pot synthesis of gold nanoparticles and application in chemotherapy of wild and resistant type visceral leishmaniasis. Colloids Surf. B Biointerfaces 107, 27–34.

Dong, L., Li, R., Wang, L., Lan, X., Sun, H., Zhao, Y., Wang, L., 2021. Green synthesis of platinum nanoclusters using lentinan for sensitively colorimetric detection of glucose. Int. J. Biol. Macromol. 172, 289–298.

Eaton, P., Quaresma, P., Soares, C., Neves, C., de Almeida, M.P., Pereira, E., West, P., 2017. A direct comparison of experimental methods to measure dimensions of synthetic nanoparticles. Ultramicroscopy 182, 179–190.

Evans, W.C., 2002. Textbook of Pharmacognosy, 683. Bailliere Tindall, London.

Fan, L., Ji, X., Lin, G., Liu, K., Chen, S., Ma, G., Xue, W., Zhang, X., Wang, L., 2021. Green synthesis of stable platinum nanoclusters with enhanced peroxidase-like activity for sensitive detection of glucose and glutathione. Microchem. J. 166, 106202.

Gardea-Torresdey, J.L., Parsons, J.G., Gomez, E., Peralta Videa, J., Troiani, H.E., Santiago, P., Yacaman, M.J., 2002. formation and growth of Au nanoparticles inside live alfalfa plants. Nano Lett. 2, 397–401.

Ghramh, H.A., Khan, K.A., Ibrahim, E.H., 2019. Biological activities of Euphorbia peplus leaves ethanolic extract and the extract fabricated gold nanoparticles (AuNPs). Molecules 24 (7), 1431.

Haugaard, N., Haugaard, E.S., 1970. Stimulation of glucose utilization by thioctic acid in rat diaphragm incubated *in vitro*. Biochim. Biophys. Acta 222, 583–586.

Iyer, R.I., Panda, T., 2018. Biosynthesis of gold and silver nanoparticles using extracts of callus cultures of pumpkin (*Cucurbita maxima*). J. Nanosci. Nanotechnol. 18, 5341–5353.

Jadhav, R., Puchchakayala, G., 2012. Hypoglycemic and antidiabetic activity of flavonoids: boswellic acid, ellagic acid, quercetin, rutin on streptozotocin-nicotinamide induced type 2 diabetic rats. Int. J. Pharm. Pharmaceut. Sci. 4, 251–256.

Jain, P.K., Lee, K.S., El-Sayed, I.H., El-Sayed, M.A., 2006. Calculated absorption and scattering properties of gold nanoparticles of different size, shape, and composition: applications in biological imaging and biomedicine. J. Phys. Chem. B 110 (14), 7238–7248.

Jia, L., Zhang, Q., Li, Q., Song, H., 2009. The biosynthesis of palladium nanoparticles by antioxidants in *Gardenia jasminoides* ellis: long lifetime nanocatalysts for p-nitrotoluene hydrogenation. Nanotechnology 20, 385601.

Khan, I., Saeed, K., Khan, I., 2019. Nanoparticles: properties, applications and toxicities. Arab. J. Chem. 12 (7), 908–931.

Khandel, P., Yadaw, R.K., Soni, D.K., Kanwar, L., Shahi, S.K., 2018. Biogenesis of metal nanoparticles and their pharmacological applications: present status and application prospects. J. Nanostruct. Chem. 8, 217–254.

Khoshnamvand, M., Hao, Z., Huo, C., Liu, J., 2020. Photocatalytic degradation of 4-nitrophenol pollutant and *in vitro* antioxidant assay of gold nanoparticles synthesized from *Apium graveolens* leaf and stem extracts. Int. J. Environ. Sci. Technol. 17 (4), 2433–2442.

Kooti, W., Ali-Akbari, S., Asadi-Samani, M., Ghadery, H., Ashtary-larky, D., 2015. A review on medicinal plant of *Apium graveolens*. Adv. Herb. Med. 1, 48–59.

Kralik, M., 2014. Adsorption, chemisorption, and catalysis. Chem. Pap. 68, 1625–1638.

Lankatillake, C., Huynh, T., Dias, D.A., 2019. Understanding glycaemic control and current approaches for screening antidiabetic natural products from evidence-based medicinal plants. Plant Methods 15, 105.

Lee, J.H., Choi, S.U.S., Jang, S.P., Lee, S.Y., 2012. Production of aqueous spherical gold nanoparticles using conventional ultrasonic bath. Nanoscale Res. Lett. 7, 420–427.

Lee, K.X., Shameli, K., Yew, Y.P., Teow, S.Y., Jahangirian, H., Rafiee-Moghaddam, R., Webster, T.J., 2020. Recent developments in the facile bio-synthesis of gold nanoparticles (AuNPs) and their biomedical applications. Int. J. Nanomed. 15, 275–300.

Levchenko, L.A., Golovanova, S.A., Lariontseva, N.V., Sadkov, A.P., Voilov, D.N., Shul'ga, YuM., Nikitenko, N.G., Shestakov, A.F., 2011. Synthesis and study of gold nanoparticles stabilized by bioflavonoids. Russ. Chem. Bull. 60, 426–433.

Li, Z., Yang, R., Yu, M., Bai, F., Li, C., Wang, Z.L., 2008. Cellular level biocompatibility and biosafety of ZnO nanowires. J. Phys. Chem. C 112, 20114–20117.

Liu, X.H., Bauman, W.A., Cardozo, C.P., 2018. Myostatin inhibits glucose uptake via suppression of insulin-dependent and -independent signaling pathways in myoblasts. Phys. Rep. 17, e13837.

Mahitha, B., Raju, B.D.P., Madhavi, T., Durga, C.H.N., Sushma, N.J., 2013. Evaluation of antibacterial efficacy of phyto fabricated gold nanoparticles using Bacopa Monniera Plant Extract. Indian J. Adv. Chem. Sci. 1 (2), 94–98.

Mai, X., Tran, M., Hoang, A., Nguyen, P., Nguyen, T., Tran, H., Nguyen, P., 2021. Gold nanoparticles from *Celastrus hindsii* and HAuCl4: green synthesis, characteristics, and their cytotoxic effects on HeLa cells. Green Process. Synth. 10 (1), 73–84.

Majidi, F.S., Mohammadi, E., Mehravi, B., Nouri, S., Ashtari, K., Neshasteh-Riz, A., 2019. Investigating the effect of near infrared photo thermal therapy folic acid conjugated gold nano shell on melanoma cancer cell line A375. Artif. Cells Nanomed. Biotechnol. 47 (1), 2161–2170.

Mezeyová, I., Hegedűsová, A., Mezey, J., Šlosár, M., Farkaš, J., 2018. Evaluation of quantitative and qualitative characteristics of selected celery (*Apium graveolens* var. Dulce) varieties in the context of juices production. Potravin. Potr. S. J. F. 12, 173–179.

Mokashi, P., Khanna, A., Pandita, N., 2017. Flavonoids from *Enicostema littorale blume* enhances glucose uptake of cells in insulin resistant human liver cancer (HepG2) cell line via IRS-1/PI3K/Akt pathway. Biomed. Pharmacother. 90, 268–277.

Moleiro, A.F., Conceição, G., Leite-Moreira, A.F., Rocha-Sousa, A., 2017. A critical analysis of the available *in vitro* and *ex vivo* methods to study retinal angiogenesis. J. Ophthalmol. 2017, 3034953.

Moreno-Álvarez, S.A., Martínez-Castañón, G.A., Niño, N., Reyes-Macías, J.F., Patiño-Marín, N., Loyola-Rodriguez, J.P., Ruiz, F., 2010. Preparation and bactericide activity of gallic acid stabilized gold nanoparticles. J. Nanoparticle Res. 12, 2741–2746.

Mosmann, T., 1983. Rapid colorimetric assay for cellular growth and survival: application to proliferation an cytotoxicity assays. J. Immunol. Methods 65 (1-2), 55–63.

Mutha, R.E., Tatiya, A.U., Surana, S.J., 2021. Flavonoids as natural phenolic compounds and their role in therapeutics: an overview. Futur. J. Pharm. Sci. 7 (1), 25.

Nayem, S.M.A., Sultana, N., Haque, M.A., Miah, B., Hasan, M.M., Islam, T., Hasan, M.M., Awal, A., Uddin, J., Aziz, M.A., Ahammad, A.J.S., 2020. Green synthesis of gold and silver nanoparticles by using *Amorphophallus paeoniifolius* tuber extract and evaluation of their antibacterial activity. Molecules 25 (20), 4773.

Naz, S., Khaskheli, A.R., Aljabour, A., Kara, H., Talpur, F.N., Sherazi, S.T.H., Khaskheli, A.A., Jawaid, S., 2014. Synthesis of highly stable cobalt nanomaterial using gallic acid and its application in catalysis. Adv. Chem. 2014, 1–7.

Nemamcha, A., Rehspringer, J.L., Khatmi, D., 2006. Synthesis of palladium nanoparticles by sonochemical reduction of palladium (II) nitrate in aqueous solution. J. Phys. Chem. B 110, 383–387.

Omolaja, A.A., Brendon, P., Omoruyia, S.I., Badmus, J.A., Ismail, E., Marnewick, J.L., Botha, S., Benjeddou, M., Ekpob, O.E., Hussein, A.A., 2021. The potential of chalcone-capped gold nanoparticles for the management of diabetes mellitus. Surface. Interfac. 2, 101251.

Oueslati, M.H., Tahar, L.B., Harrath, A.H., 2020. Catalytic, antioxidant and anticancer activities of gold nanoparticles synthesized by kaempferol glucoside from *Lotus leguminosae*. Arab. J. Chem. 13, 3112–3122.

Pamies, R., Cifre, J.G.H., Espín, V.F., Francisco, M.G., Banos, G.D., Torre, J.G., 2014. Aggregation behaviour of gold nanoparticles in saline aqueous media. J. Nanoparticle Res. 16, 2376.

Parimalam, S., Badilescu, S., Bhat, R., Packirisamy, M.A., 2020. Narrative review of scientific validation of gold- and silver-based Indian medicines and their future scope. Longhua Chin. Med. 3, 2020. https://lcm.amegroups.com/article/view/6464.

Patra, J.K., Das, G., Fraceto, L.F., Campos, E.V.R., Rodriguez-Torres, M.D.P., Acosta-Torres, L.S., Diaz-Torres, L.A., Grillo, R., Swamy, M.K., Sharma, S., Habtemariam, S., Shin, H.S., 2018. Nano based drug delivery systems: recent developments and future prospects. J. Nanobiotechnol. 16 (1), 71.

Prasathkumar, M., Anisha, S., Dhrisya, C., Becky, R., Sadhasivam, S., 2021. Therapeutic and pharmacological efficacy of selective Indian medicinal plants – a review. Phytomedicine 1 (2), 100029.

Rebollo-Hernanz, M., Zhang, Q., Aguilera, Y., Martín-Cabrejas, M.A., Gonzalez de Mejia, E., 2019. Cocoa shell aqueous phenolic extract preserves mitochondrial function and insulin sensitivity by attenuating inflammation between macrophages and adipocytes *in vitro*. Mol. Nutr. Food Res. 63, 1801413.

Rodrigues, F.A., Bomfim Ida, S., Cavalcanti, B.C., Pessoa, C., Goncalves, R.S., Wardell, J.L., Wardell, S.M., de Souza, M.V., 2014. Mefloquine-oxazolidine derivatives: a new class of anticancer agents. Chem. Biol. Drug Des. 83 (1), 126–131.

Sadalage, P.S., Patil, R.V., Havaldar, D.V., Gavade, S.S., Santos, A.C., Pawar, K.D., 2021. Optimally biosynthesized, PEGylated gold nanoparticles functionalized with quercetin and camptothecin enhance potential anti-inflammatory, anti-cancer and anti-angiogenic activities. J. Nanobiotechnol. 19 (1), 84.

Santhoshkumar, J., Rajeshkumar, S., Venkat Kumar, S., 2017. Phyto-assisted synthesis, characterization and applications of gold nanoparticles - a review. Biochem. Biophys. Rep. 11, 46–57.

Selvakumar, T.A., Rajasekar, P., 2017. *Aerva lanata* mediated phytofabrication of silver nanoparticles and evaluation of their antibacterial activity against wound associated bacteria. J. Taiwan Inst. Chem. Eng. 78, 539–551.

Sett, A., Gadewar, M., Sharma, P., Deka, M., Bora, U., 2016. Green synthesis of gold nanoparticles using aqueous extract of *Dillenia indica*. Adv. Nat. Sci. Nanosci. Nanotechnol. 7, 025005.

Shen, F.W., Zhou, K.C., Cai, H., Zhang, Y.N., Zheng, Y.L., Quan, J., 2019. One-pot synthesis of thermosensitive glycopolymers grafted gold nanoparticles and their lectin recognition. Colloids Surf. B Biointerfaces 173, 504–511.

Shivashri, C., Rajarajeshwari, T., Rajasekar, P., 2013. Hepatoprotective action of celery (*Apium graveolens*) leaves in acetaminophen-fed freshwater fish (*Pangasius sutchi*). Fish Physiol. Biochem. 39, 1057–1069.

Singh, R., Lillard Jr., J.W., 2009. Nanoparticle-based targeted drug delivery. Exp. Mol. Pathol. 86 (3), 215–223.

Sofowora, A., 1993. Screening Plants for Bioactive Agents, Medicinal Plants and Traditional Medicine in Africa, 134. Spectrum Books Ltd, Nigeria.

Sulaiman, G.M., Waheeb, H.M., Jabir, M.S., Khazaal, S.H., Dewir, Y.H., Naidoo, Y., 2020. Hesperidin loaded on gold nanoparticles as a drug delivery system for a successful biocompatible, anti-cancer, anti-inflammatory and phagocytosis inducer model. Sci. Rep. 10 (1), 9362.

Sunderam, V., Thiyagarajan, D., Lawrence, A.V., Mohammed, S.S.S., Selvaraj, A., 2019. *In-vitro* antimicrobial and anticancer properties of green synthesized gold nanoparticles using *Anacardium occidentale* leaves extract. Saudi J. Biol. Sci. 26, 455–459.

Templeton, A.C., Pietron, J.J., Murray, R.W., Mulvaney, P., 2000. Solvent refractive index and core charge influences on the surface plasmon absorbance of alkanethiolate monolayer-protected gold clusters. J. Phys. Chem. B 104 (3), 564–570.

Thanganadar Appapalam, S., Paul, B., Arockiasamy, S., Panchamoorthy, R., 2020. Phytofabricated silver nanoparticles: discovery of antibacterial targets against diabetic foot ulcer derived resistant bacterial isolates. Mater. Sci. Eng. C. Mater. Biol. Appl. 117, 111256.

Vijayakumar, S., Ganesan, S., 2012. *In vitro* cytotoxicity assay on gold nanoparticles with different stabilizing agents. J. Nanomater. 2012, 1–9.
Wang, C., 1985. Insulin-stimulated glucose uptake in rat diaphragm during postnatal development: lack of correlation with the number of insulin receptors and of intracellular glucose transporters. Proc. Natl. Acad. Sci. Unit. States Am. 82, 3621-3265.
Wang, W., Chen, Q., Jiang, C., Yang, D., Liu, X., Xu, S., 2007. One-step synthesis of biocompatible gold nanoparticles using gallic acid in the presence of poly-(N- vinyl-2-pyrrolidone). Colloids Surf. A Physicochem. Eng. Asp. 301, 73–79.
Wang, T., Wang, J., Hu, X., Huang, X.J., Chen, G.X., 2020. Current understanding of glucose transporter 4 expression and functional mechanisms. World J. Biol. Chem. 11 (3), 76–98.
Wang, Y., Quinsaat, J.E.Q., Ono, T., Maeki, M., Tokeshi, M., Isono, T., Tajima, K., Satoh, T., Sato, S.I., Miura, Y., Yamamoto, T., 2020b. Enhanced dispersion stability of gold nanoparticles by the physisorption of cyclic poly(ethylene glycol). Nat. Commun. 11 (1), 6089.
Zhang, X., Servos, M.R., Liu, J.W., 2012. Ultrahigh nanoparticle stability against salt, pH, and solvent with retained surface accessibility via depletion stabilization. J. Am. Chem. Soc. 134, 9910–9913.
Zhao, L., Wang, Y., Zhao, X., Deng, Y., Li, Q., Xia, Y., 2018. Green preparation of ag-au bimetallic nanoparticles supported on graphene with alginate for non-enzymatic hydrogen peroxide detection. Nanomaterials 8 (7), 507.
Zhou, K., Zhao, F., Liu, Z., Zhuang, Y., Chen, L., Qiu, F., 2009. Triterpenoids and flavonoids from celery (*Apium graveolens*). J. Nat. Prod. 72, 1563–1567.
Zierath, J.R., Henriksson, H.W., 2003. Muscle Metabolism. Taylor & Francis, New York.